SITELLE, CFHT's wide-field imaging Fourier transform spectrometer: from the Milky way to clusters of galaxies

Laurent Drissen[a], the SITELLE Team[a,b,c,d,e], and the SIGNALS Collaboration[a,d,e,f]

[a]Département de physique, de génie physique et d'optique, Université Laval, Québec, Canada
[b]ABB Analytical, Québec, Canada
[c]Département de Physique, Université de Montréal, Montréal, Canada
[d]Canada-France-Hawaii Telescope, Kamuela, HI, USA
[e]University of Hawaii, Hilo, HI, USA
[f]Laboratoire d'astrophysique de Marseille, Marseille, France

ABSTRACT

We present a technical and scientific overview of SITELLE, an imaging Fourier transform spectrometer in the visible band installed at the Canada-France-Hawaii telescope, and highlight some of its most interesting results, from nearby nebulae to clusters of galaxies. SITELLE represents a total incongruity in the world of Fourier transform spectroscopy, being used in the visible range down to 350 nm, presenting a large field of view ($11'' \times 11''$) and collecting more than four million spectra per data cube. Among its noteworthy achievements, SITELLE obtained the first realistic 3D views of the AT Cnc dwarf nova ejecta and of the Crab supernova remnant, a unique collection of emission line maps of a large sample of nearby galaxies, as well as the detection of ram pressure effects on star-forming galaxies in a cluster 3 billion light-years from us.

Keywords: Fourier transform spectroscopy, emission-line nebulae, star-forming galaxies

1. INTRODUCTION

Seven years after its commissionning, this SPIE meeting is a good opportunity to present an overview of SITELLE, a visible-band imaging Fourier transform spectrometer (iFTS) installed at the Canada-France-Hawaii telescope (CFHT) and highlight some of its scientific achievements. In the world of Fourier transform spectroscopy (in astronomy and other applications), SITELLE is a clear outlier because it performs in the visible range, in filter-selected bandpasses from 350 nm to 850 nm. It also harbors a wide field of view ($11'' \times 11''$), sampled at $0.32''$/pixel, therefore producing more than four million spectra per data cube, with a resolution up to R$\sim 10^4$ (see Table 1). While the science lead,[1] optical design,[2] and its integration were done at Université Laval, its mechanical design and fabrication of the input and output optics at Université de Montréal, most of the design[3] and construction work has been performed by ABB Analytical, a Québec-based company specialized in Fourier transform spectrometers and optical sensors. CFHT[4] took the responsibility of the detectors' enclosure and cooling system.

SITELLE is also an outlier in the integral field spectroscopy (IFS) zoo[5] because it does not rely upon dispersive elements to extract spectral information from its targets, but rather on an off-axis Michelson interferometer. This presents some disadvantages compared to dispersive IFS such as MUSE,[6] especially in the study of absorption-line sources, but its wide field of view (121 times larger than MUSE), high efficiency in the blue-violet region and relatively low cost make it an instrument of choice for a variety of astronomical targets such as Galactic nebulae, nearby galaxies and more distant clusters of galaxies, which will be discussed in sections 3,4 and 5.

Further author information: E-mail: ldrissen@phy.ulaval.ca, Telephone: 1 418 656 2131 ext 405641

Table 1. SITELLE Characteristics.

Field of view	$11' \times 11'$
Pixel size	$0.32''$
Detectors (2)	Deep depletion e2v CCDs (2048×2064)
Spectral resolution	1 - 10 000
Wavelength range	350 - 900 nm
Filters bandwidth	23 nm (SN1) to 95 nm (C1)

2. DATA ACQUISITION, SOFTWARE AND CALIBRATION

2.1 Data acquisition

Deep-depletion e2v CCDs collect two complementary interferograms of the sources at the output ports of the interferometer through a series of images obtained at different Optical Path Difference (OPD) positions. The spectral resolution depends on the maximum OPD reached during the data acquisition, hence on the number of mirror steps (typically a few hundred). Total acquisition times for data cubes vary between 1 and 4 hours, with individual exposures at each mirror step lasting a few seconds to one minute; the overhead required to move and stabilize the mirror and simultaneously read the CCDs amount to 3.8 seconds per step. The longest data cubes are often obtained over the course of two or three nights in order to minimize the airmass or maximize the overall schedule of an observing run; this does not affect much the quality of the data compared with single-night observations, thanks to the very accurate determination of the mirror positions. A single spectral data cube, weighting between 2 and 30 Gb depending on the spectral resolution, is then obtained through Fourier transforms.

Medium and wide-band filters are used to acquire the data in order to minimize the shot noise and maximize the spectral resolution for a given acquisition time. Characteristics of these filters are presented in Figure 1. All filters have been provided by Custom Scientific; they have very flat transmission curves with sharp edges. Most of the visible range is covered with the current filter set. The SN filter series is intended to determine the properties of HII regions of the Milky Way and nearby galaxies using strong emission lines, while the C series aims at fainter lines in HII regions, absorption lines in stars and nearby galaxies, as well a the detection of emission line galaxies in low-redshift clusters. Filter SN3 is SITELLE's workhorse because it includes the bright Hα line along with a series of important diagnostic emission lines.

We finally note that while the Fourier transform of the interferograms produces a spectral cube, their sum creates a deep image corresponding to the integral flux within the filter bandpass.

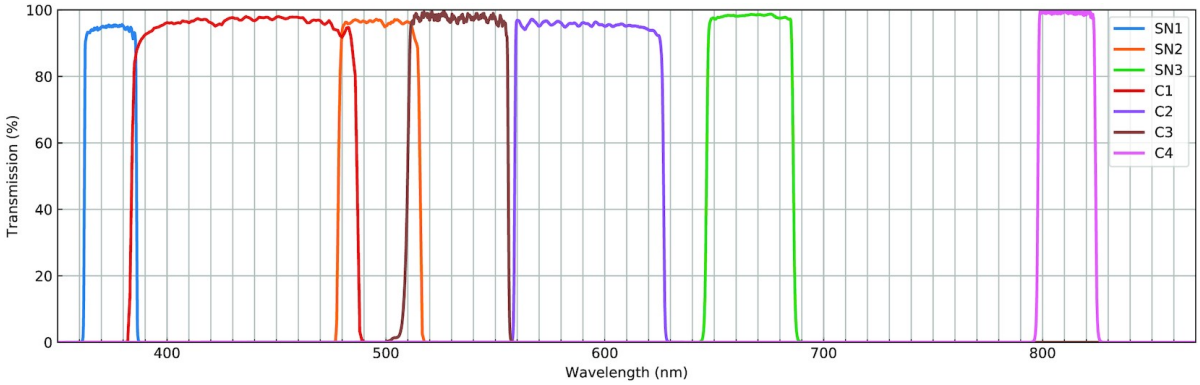

Figure 1. Transmission curves of SITELLE filters.

2.2 Software and data products

The complexity of an instrument like SITELLE makes the design of dedicated data reduction and analysis software a fundamental component of the system. We have put considerable efforts on the development of ORBS,[7,8] a fully automated data reduction pipeline, as well as in ORCS[9*], a fitting engine for a fast and reliable extraction of the spectral parameters. Both are updated on a regular basis to improve the quality of the data product and to adapt to the needs of the observers. The data reduction process with ORBS is quite complex since it involves, in addition to the usual CCD frames reduction, the alignment of the two interferometric cubes, computation of the 3D phase corrections, Fourier transforms and spectral as well as photometric calibrations. The outcome of this process is a calibrated spectral data cube, in hdf5 format, that can easily be transformed into fits format to be displayed by a viewing software such as ds9. Note that the natural spectral units of an FTS are wavenumbers (cm^{-1}), so for astronomers used to wavelengths (nanometers or Angströms), SITELLE spectra might look awkward at first sight, with spectral lines in reverse order; but one gets used to it! ORCS then uses this hdf5 file as input to extract and fit integrated spectra of selected regions (Figure 2), or produce maps of line fluxes, velocity and velocity dispersion as well as their uncertainties.

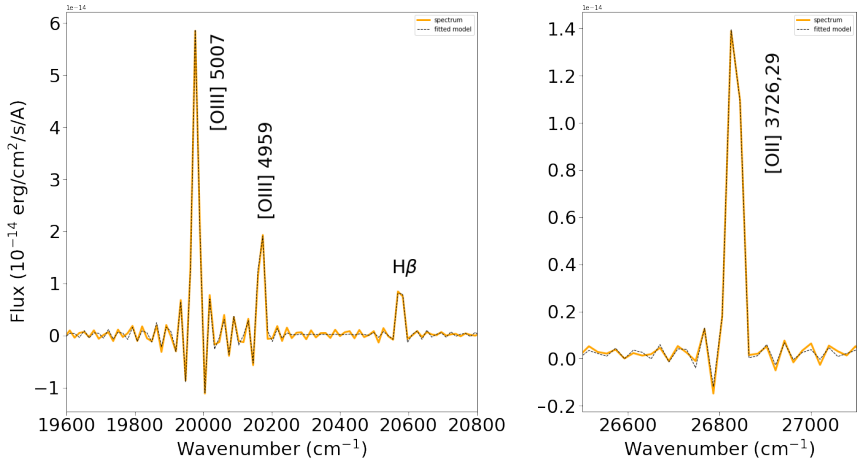

Figure 2. Integrated spectrum of an HII region in M33 (radius of 20 pixels) in the SN2 and SN1 filter. The observations are in orange, while a fit with ORCS to measure the line flux, velocity and velocity dispersion, is shown as dotted black lines.

Figure 2 shows the integrated spectrum of a nebula ionized by hot massive stars in the spiral galaxy M33, in the spectral range covered by filters SN2 and SN1, along with a fit with ORCS superimposed on the data. The first thing to notice is SITELLE's instrument line shape (ILS) which is, as for all FTS, a sinc function. Moving through a given data cube can therefore be troubling since regions with negative flux appear on each side of a maximum, corresponding to the minima of the sinc sidelobes. Any movement of the ionized gas along the line of sight, caused for example by a systematic expansion (as for a supernova remnant), turbulent motion due to the presence of stellar winds, or simply the superposition of unrelated filaments along the line of sight will result in a convolution of this sinc function with a gaussian. The so-called sincgauss function was therefore introduced in ORCS to take this into account.[10] Figure 3 shows the result of three fits to the integrated spectra of nebulae in an external galaxy with different values of the velocity dispersion, parameterized by σ. The brightest line is Hα, with the [NII] 6548,84 doublet on its sides. One clearly see the sidelobes of the sinc function on the left panel, with a very low value of σ. The sidelobes' amplitude diminishes as the velocity dispersion increases and becomes negligible in the spectrum on the right panel, which actually represents a supernova remnant.

Recently, another data analysis package specifically geared toward SITELLE data using machine learning, LUCI,[11] has been developped to study the HII region kinematics[12,13] and line ratios.[14]

*https://orcs.readthedocs.io/en/latest/

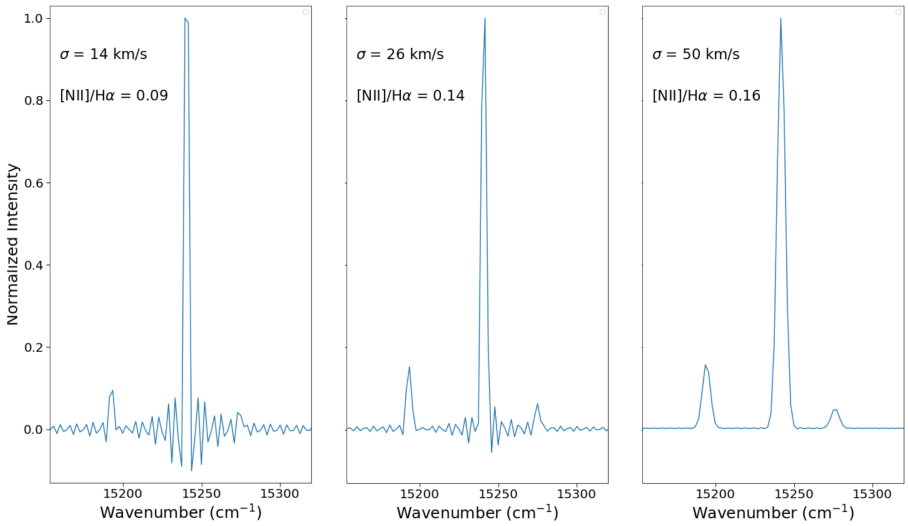

Figure 3. Fits to the spectra of three HII regions (Hα and [NII] lines) in M33 emphasizing the change in line shape as the velocity dispersion along the line of sight increases. The spectrum in the left panel is indistinguishable from the instrument ILS (a sinc function) whereas the right panel, showing the spectrum of a supernova remnant, is very similar to that obtained with dispersive spectrographs, dominated by a gaussian ILS.

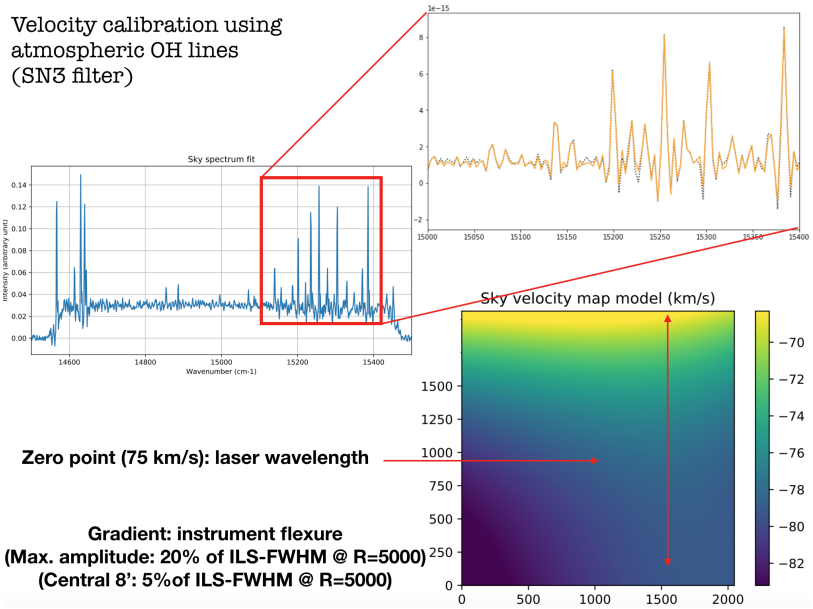

Figure 4. Wavelength calibration using the night-sky OH lines.

2.3 Wavelength calibrations

A recent paper[8] describes in great details the photometric, spectroscopic and astrometric calibrations involved in the data reduction. We just want to add a few words here specifically about the wavelength calibration. Contrary to conventional dispersive spectroscopy, for which wavelength calibration using arcs can be obtained quickly with the telescope pointing at the source, obtaining a calibration datacube with SITELLE takes significantly more time. Therefore, zero-point wavelength calibrations are obtained with a laser data cube pointing at the zenith, at the end of the night.The exact wavelength of the laser being itself not known with an absolute precision,

and the instrument flexure causing variations of the zero-point across the field of view, night-sky emission lines (mostly from the OH molecule) within the data cubes (in the SN1, SN3, C2 and C4 filters) are used to improve the wavelength calibration, and hence the velocity fields of the targets with a precision of 1 - 3 km s^{-1} from opposite sides of the field of view (see Fig. 4).

Some early examples of SITELLE's science capabilities were presented elsewhere;[1] the next sections present a review of its more recent scientific highlights.

3. MILKY WAY

Extended emission-line objects such as nebulae in the Milky Way are targets of choice for SITELLE. It is interesting to note that although some of them are easy targets for amateur astronomers, they have not been studied in great detail with modern instruments such as integral field spectrographs on professional telescopes. The structure of planetary nebulae (M27[10] for instance), wind-blown bubbles around massive stars (M1-67[15] or NGC 6888 - see Ruest et al., these proceedings), or ejecta from old nova eruptions (AT Cnc[16]) have all benefited from SITELLE's wide field.

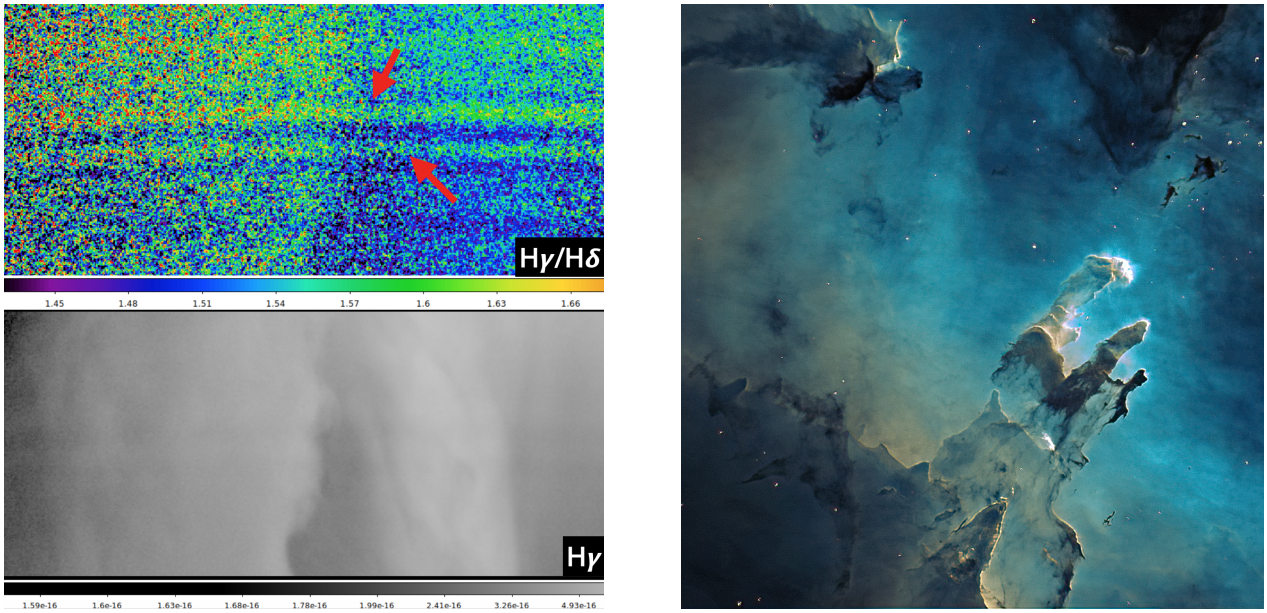

Figure 5. (Left) Hγ map of a $3' \times 1.5'$ field in the center of the Orion nebula (bottom) and the Hγ / $H\delta$ ratio map (top). Arrows point to artefacts caused by an erroneous phase correction of the interferograms. (Right) Composite image of the M16 nebula from a SITELLE SN3 cube, with the [NII] 6584 coded in blue and Hα in red.

Ironically, one of the brightest and extended HII regions of our galaxy, the Orion nebula, proved to be a difficult target for SITELLE: the total absence of continuum in the field of view rendered the determination of the interferometric phase correction very difficult, resulting in a distorted ILS and non-negligible ($\sim 5 - 8\%$) artefacts in some line ratio maps (Figure 5, left panel). Similar artefacts were noticed in velocity maps by Flagey[17] and collaborators, who have presented a very detailed study of the "Pillars of Creation" nebula, M16 (Figure 5, right panel) and some of its components using the SN1, SN2 and SN3 filters. They have however noticed an excellent agreement with line fluxes obtained with MUSE and HST.

The three-dimensional structure of supernova remnants is another field of research in which SITELLE can make significant contributions. Despite a very modest spectral resolution (R = 1500), Alarie & Drissen[18] were able to disentangle the approaching and receding sides of IC 443, separated by less than 100 km s^{-1}. This was made possible by the excellent accuracy with which the instrument ILS is known and ORCS's capability to fit multiple components. In supernova remnants, the forbidden lines are almost as intense as Hα, thus significantly

improving the precision in the measurement of velocities. This work revealed very different morphological structures probably caused by variations in the density properties of the interstellar medium in which this old supernova remnant has been interacting.

The highlight of SITELLE's supernova remnant work is the first realistic 3D reconstruction of the Crab nebula,[19] which was made possible by the highest spectral resolution on-sky data cube obtained with the SN3 filter, R = 8870. This was short (by 8%) of the intended spectral resolution (R = 9600), very likely due to the decrease in modulation efficiency of the Michelson interferometer at large values of optical path difference.

A similar study, on a large number of supernova remnants but with much less spatial resolution, is underway in the nearby spiral galaxy M33 (Duarte-Puertas et al., in prep.).

4. NEARBY GALAXIES

Star-forming, nearby galaxies (up to 100 Mpc) are, by far, SITELLE's main targets. Some recent noteworthy publications include a study of a sample of spirals to search for kinematic signatures of late gas accretion,[20] a detailed chemical and kinematic investigation of the interacting pair Arp 82 supplemented by numerical simulations,[21] and an investigation of the star-formation efficiency in the AGN-host galaxy NGC 3169 using both SITELLE and ALMA data.[22]

SIGNALS[23†], a recently completed CFHT Large Program led by Laurie Rousseau-Nepton, aims at studying the properties of more than 30 000 HII regions in a sample of three dozen nearby galaxies, using the SN1 (R = 1000), SN2 (R = 1000) and SN3 (R = 5000) filters. Local Group galaxies in this work, for which individual stars can be distinguished from the ground or with HST, include M31 (5 pointings), M33 (9 pointings - see Figure6), NGC 6822, WLM, IC 1613 and Sextans A (one pointing each). Data on these nearby, well studied, galaxies allow detailed work on individual HII regions, supernova remnants (Duarte-Puertas et al., in preparation), planetary nebulae and wind-blown bubbles around individual massive stars (Tuquet et al., submitted to MNRAS) that can then be used to interpret the data on more distant galaxies in the SIGNALS sample (the majority of them are at distances of 3 - 9 Mpc).

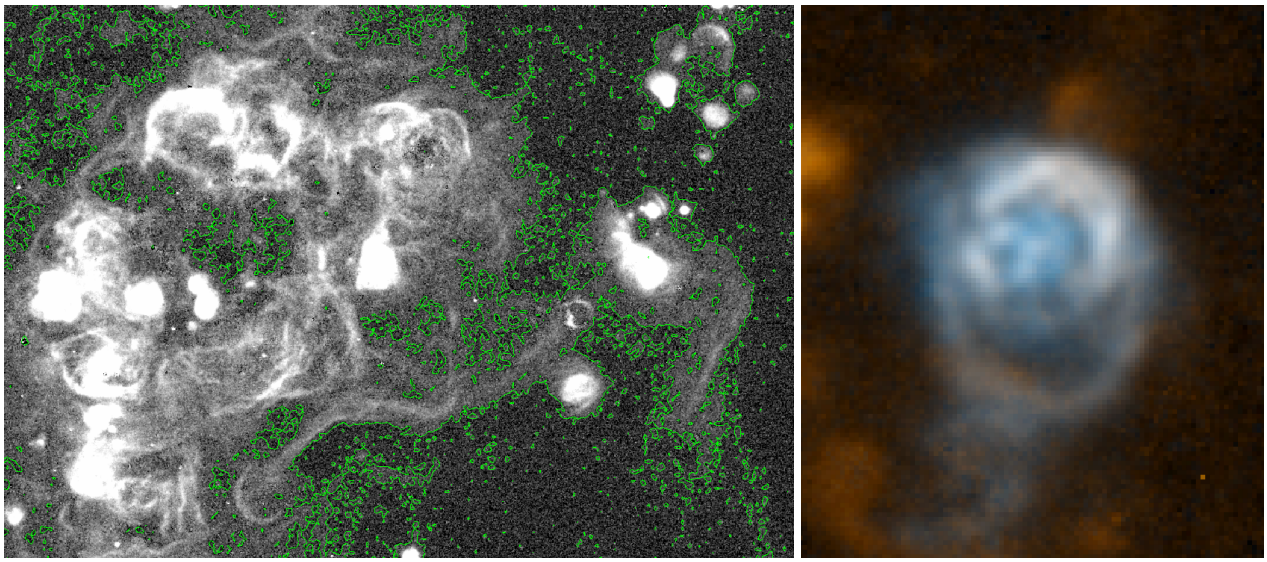

Figure 6. (Left) Hα map of a $4.7' \times 3.4'$ field M33 extracted from a 4 hour, R = 5000 SN3 data cube. Green contours indicate a flux of 4×10^{-18} erg cm^{-2} s^{-1} pixel^{-1}. (Right) Color composite (orange = Hα, blue = [OIII] 5007) of the WR wind-blown bulle F4-1 in the same galaxy; the bright, round section of the bubble has a diameter of 40 parsecs.

Figure 6 (left panel) shows the Hα flux map of a region in the south of the spiral galaxy M33 along with contours indicating the detection limit. This threshold is identical to the expectations from the initial design of

[†]https://signal-survey.org/

SITELLE. The right-hand panel of the same figure illustrates the level of detail attainable on individual objects for the Local Group galaxies.

Pushing the limits of the iFTS technology down to the blue-violet region was a major technical challenge in terms of servo mechanism and mirror positioning. The main incentive for this requirement was to be able to map the important [OII] 3727 diagnostic line. A high enough spectral resolution (R $\leq$ 2500) allows to separate the two components of this doublet,[1] the ratio of which provides an excellent measurement of the electronic density of the ionized gas. But even at modest resolution (R = 1000 is the SIGNALS standard), mapping this line is an important diagnostic of the oxygen abundance and ionization (in conjunction with maps of the [OIII] 5007 line from the SN2 data cubes). An example is provided in Figure 7, which shows the ionized gas of low ionization swirling around the central black hole at the core of the M31 spiral galaxy. We note that the same field was also observed with the SN3 filter in the early science verification phase of SITELLE; this led to the discovery of about 800 point-like emission-line sources,[24] most of which are planetary nebulae. The same paper also introduces details of the photometric, wavelength and astrometric calibration of the SITELLE data cubes.

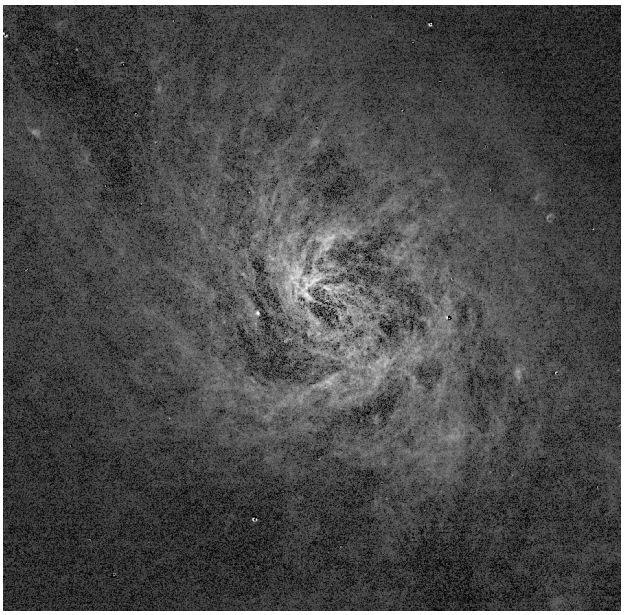

Figure 7. Central field of M31 in the light of the [OII] 3727 doublet, extracted from a 2.5 hour R = 1000 SN1 data cube.

Prior to the official start of the SIGNALS survey, some galaxies were targeted to assess SITELLE's capabilities for this area of research. This is the case of NGC 628,[25] in which more than 4000 HII regions were detected and their luminosity function determined with unprecedented accuracy. The same dataset was used as a database to test the predictions of the WARPFIELD-EMP emission-line predictor.[26] Another noteworthy example is the detailed study of properties of the supernova remnant population in NGC 3344.[27]

One of the most compelling asset of SITELLE in the study of galaxies is its ability to provide very accurate measurement of their velocity field in the Hα region, thanks to the stability of its ILS and the calibration accuracy provided by the night-sky OH lines (see section 2.3). This is illustrated in Figure 8 for the interacting pair of galaxies NGC 4490. While the global velocity maps are used to model the galaxies'dynamics, which is particularly important to diagnose and model current or past interactions,[21] the sub-km s^{-1} accuracy within HII regions, as well as the measurement of their velocity dispersion and multiple components[12] are essential to model the impact of stellar winds and supernova remnant on a local scale.

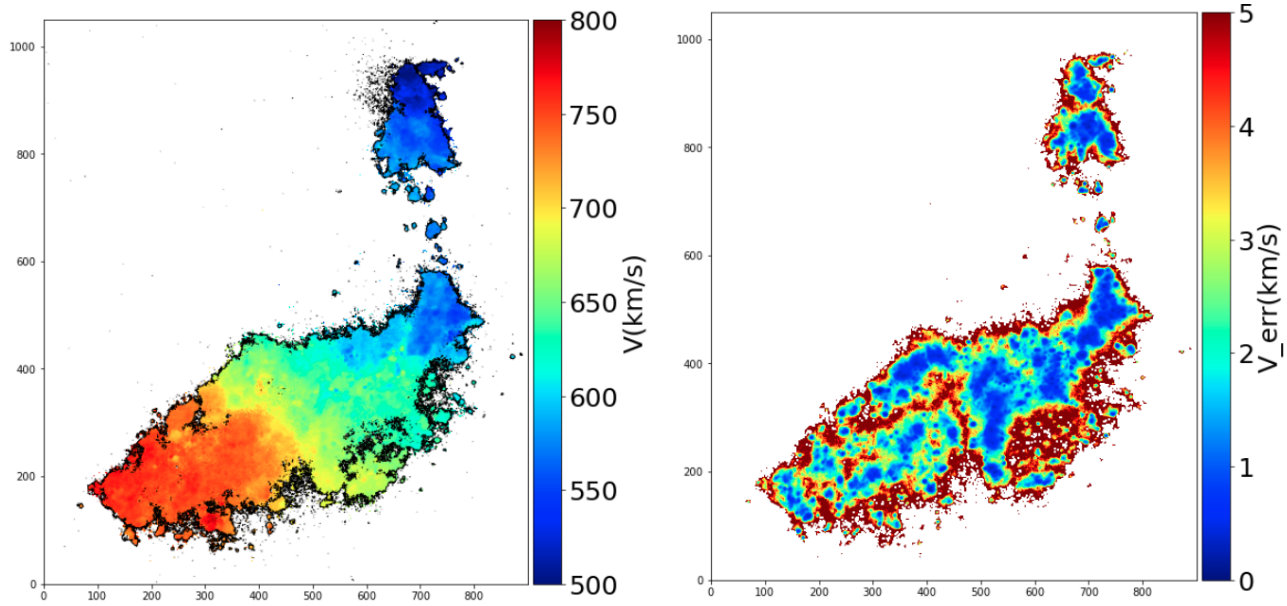

Figure 8. Velocity field and its corresponding error map for the interacting pair of galaxies NGC 4490.

5. GROUPS AND CLUSTERS OF GALAXIES, SERENDIPITY

Clusters of galaxies were part of the science drivers behind the design of SITELLE and its filter set. Duarte Puertas and collaborators have done a remarquable job at disecting the star-forming regions in Stephan's Quintet,[28,29] a tight group of interacting galaxies at a distance of 75 Mpc, using one of the first SITELLE data cube obtained during it commissioning; they even discovered a new member! At the core of the Perseus cluster at a distance of about 100 Mpc lies NGC 1275, host of an active nucleus, which is surrounded by an immense network of ionized gas filaments. Gendron-Marsolais[30] and collaborators have used SITELLE to study the kinematics of these filaments, as well as the line ratios.

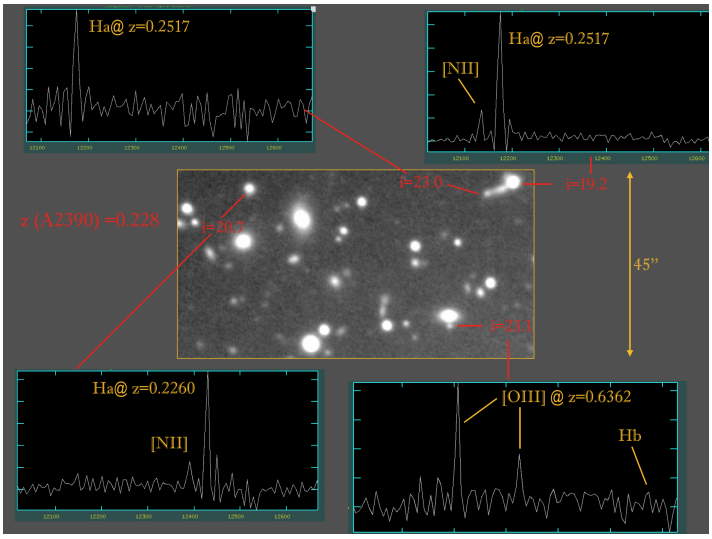

Figure 9. Small portion of the deep C4 filter image of Abell 2390 showing spectra of three member galaxies and a more distant outlier.

The C4 filter was specially designed to target galaxy clusters at a redshift of ~ 0.25 (795 - 825 nm). This spectral region is a small window between dense forests of night-sky OH lines, although some of these lines are present. A group at the University of Toronto, led by Howard Yee, and collaborators in Taiwan, have undertaken a systematic study of a sample of galaxy clusters with the C4 filter to target the Hα line, complemented by other, bluer filters. Figure 9 presents a very small region in Abell 2390, very rich in emission-line galaxies. A study of Abell 2390 and Abell 2465 by this group[31] discovered more than 100 emission-line galaxies and further showed clear offsets between the emission-line region and the continuum pointing away from the cluster centers resulting from ram pressure stripping.

Emission-line galaxies were also detected in the even more distant z $\sim$0.5 clusters Cl0016+1609 and MACS J1621+38101,[32] this time using the C2 and C3 filters to target the [OII] 3727 emission line, a good indicator of the star-formation rate.

We conclude by mentioning that background emission-line galaxies at different redshifts are almost always present in the field of SITELLE targets away from the Galactic plane. A complete inventory of these galaxies, their star-formation rate and redshift distribution could be an excellent archival project.

ACKNOWLEDGMENTS

This paper is based on data obtained with the Canada-France-Hawaii Telescope (CFHT), which is operated by the National Research Council of Canada, the Institut National des Sciences de l'Univers of the Centre National de la Recherche Scientifique of France and the University of Hawaii.The authors wish to recognize and acknowledge the very significant cultural role that the summit of Mauna Kea has always had within the indigenous Hawaiian community. We are most grateful to have the opportunity to conduct observations from this mountain. The observations were obtained with SITELLE, a joint project of Université Laval, ABB, Université de Montréal and the CFHT, with support from the Canada Foundation for Innovation, the National Sciences and Engineering Research Council of Canada (NSERC) and the Fonds de Recherche du Québec - Nature et Technologies (FRQNT). LD is grateful to NSERC and FRQNT for financial support.

REFERENCES

[1] Drissen, L., Martin, T., Rousseau-Nepton, L., Robert, C., Martin, R. P., Baril, M., Prunet, S., Joncas, G., Thibault, S., Brousseau, D., Mandar, J., Grandmont, F., Yee, H., and Simard, L., "SITELLE: an Imaging Fourier Transform Spectrometer for the Canada-France-Hawaii Telescope," **485**, 3930–3946 (May 2019).

[2] Brousseau, D., Thibault, S., Fortin-Boivin, S., Zhang, H., Vallée, P., Auger, H., and Drissen, L., "SITELLE optical design, assembly, and testing," in [*Ground-based and Airborne Instrumentation for Astronomy V*], Ramsay, S. K., McLean, I. S., and Takami, H., eds., *Society of Photo-Optical Instrumentation Engineers (SPIE) Conference Series* **9147**, 91473Z (July 2014).

[3] Grandmont, F., Drissen, L., Mandar, J., Thibault, S., and Baril, M., "Final design of SITELLE: a wide-field imaging Fourier transform spectrometer for the Canada-France-Hawaii Telescope," in [*Ground-based and Airborne Instrumentation for Astronomy IV*], McLean, I. S., Ramsay, S. K., and Takami, H., eds., *Society of Photo-Optical Instrumentation Engineers (SPIE) Conference Series* **8446**, 84460U (Sept. 2012).

[4] Baril, M. R., Grandmont, F. J., Mandar, J., Drissen, L., Martin, T., Rousseau-Nepton, L., Thibault, S., Brousseau, D., Levesque, S. R., Thomas, J., Malo, L., Morrison, G., le Gal, M., Jones, W., Barrick, G., Benedict, T., Salmon, D., Prunet, S., and Devost, D., "Commissioning SITELLE: an imaging Fourier transform spectrometer for the Canada France Hawaii Telescope," in [*Ground-based and Airborne Instrumentation for Astronomy VI*], Evans, C. J., Simard, L., and Takami, H., eds., *Society of Photo-Optical Instrumentation Engineers (SPIE) Conference Series* **9908**, 990829 (Aug. 2016).

[5] Maillard, J. P., Drissen, L., Grandmont, F., and Thibault, S., "Integral wide-field spectroscopy in astronomy: the Imaging FTS solution," *Experimental Astronomy* **35**, 527–559 (Apr. 2013).

[6] Bacon, R., Accardo, M., Adjali, L., Anwand, H., Bauer, S., Biswas, I., Blaizot, J., Boudon, D., Brau-Nogue, S., Brinchmann, J., Caillier, P., Capoani, L., Carollo, C. M., Contini, T., Couderc, P., Daguisé, E., Deiries, S., Delabre, B., Dreizler, S., Dubois, J., Dupieux, M., Dupuy, C., Emsellem, E., Fechner, T., Fleischmann, A., François, M., Gallou, G., Gharsa, T., Glindemann, A., Gojak, D., Guiderdoni, B., Hansali, G., Hahn, T.,

Jarno, A., Kelz, A., Koehler, C., Kosmalski, J., Laurent, F., Le Floch, M., Lilly, S. J., Lizon, J. L., Loupias, M., Manescau, A., Monstein, C., Nicklas, H., Olaya, J. C., Pares, L., Pasquini, L., Pécontal-Rousset, A., Pelló, R., Petit, C., Popow, E., Reiss, R., Remillieux, A., Renault, E., Roth, M., Rupprecht, G., Serre, D., Schaye, J., Soucail, G., Steinmetz, M., Streicher, O., Stuik, R., Valentin, H., Vernet, J., Weilbacher, P., Wisotzki, L., and Yerle, N., "The MUSE second-generation VLT instrument," in [*Ground-based and Airborne Instrumentation for Astronomy III*], McLean, I. S., Ramsay, S. K., and Takami, H., eds., *Society of Photo-Optical Instrumentation Engineers (SPIE) Conference Series* **7735**, 773508 (July 2010).

[7] Martin, T., Drissen, L., and Joncas, G., "ORBS: A data reduction software for the imaging Fourier transform spectrometers SpIOMM and SITELLE," in [*Software and Cyberinfrastructure for Astronomy II*], Radziwill, N. M. and Chiozzi, G., eds., *Society of Photo-Optical Instrumentation Engineers (SPIE) Conference Series* **8451**, 84513K (Sept. 2012).

[8] Martin, T., Drissen, L., and Prunet, S., "Data reduction and calibration accuracy of the imaging Fourier transform spectrometer SITELLE," **505**, 5514–5529 (Aug. 2021).

[9] Martin, T. and Drissen, L., "ORCS: a Post-processing Software for the Wide Field Imaging Fourier Transform Spectrometer SITELLE," in [*Astronomical Data Analysis Software and Systems XXVII*], Ballester, P., Ibsen, J., Solar, M., and Shortridge, K., eds., *Astronomical Society of the Pacific Conference Series* **522**, 41 (Apr. 2020).

[10] Martin, T. B., Prunet, S., and Drissen, L., "Optimal fitting of Gaussian-apodized or under-resolved emission lines in Fourier transform spectra providing new insights on the velocity structure of NGC 6720," **463**, 4223–4238 (Dec. 2016).

[11] Rhea, C., Hlavacek-Larrondo, J., Rousseau-Nepton, L., Vigneron, B., and Guité, L.-S., "LUCI: A Python Package for SITELLE Spectral Analysis," *Research Notes of the American Astronomical Society* **5**, 208 (Sept. 2021).

[12] Rhea, C., Rousseau-Nepton, L., Prunet, S., Hlavacek-Larrondo, J., and Fabbro, S., "A Machine-learning Approach to Integral Field Unit Spectroscopy Observations. I. H ii Region Kinematics," **901**, 152 (Oct. 2020).

[13] Rhea, C. L., Rousseau-Nepton, L., Prunet, S., Hlavacek-Larrondo, J., Martin, R. P., Grasha, K., Asari, N. V., Bégin, T., Vigneron, B., and Prasow-Émond, M., "A Machine-learning Approach to Integral Field Unit Spectroscopy Observations. III. Disentangling Multiple Components in H II Regions," **923**, 169 (Dec. 2021).

[14] Rhea, C., Rousseau-Nepton, L., Prunet, S., Prasow-Émond, M., Hlavacek-Larrondo, J., Asari, N. V., Grasha, K., and Perreault-Levasseur, L., "A Machine-learning Approach to Integral Field Unit Spectroscopy Observations. II. H II Region Line Ratios," **910**, 129 (Apr. 2021).

[15] Sévigny, M., St-Louis, N., Drissen, L., and Martin, T., "New insights into the WR nebula M1-67 with SITELLE," **501**, 5350–5361 (Mar. 2021).

[16] Shara, M. M., Drissen, L., Martin, T., Alarie, A., and Stephenson, F. R., "When does an old nova become a dwarf nova? Kinematics and age of the nova shell of the dwarf nova AT Cancri," **465**, 739–745 (Feb. 2017).

[17] Flagey, N., McLeod, A. F., Aguilar, L., and Prunet, S., "Wide field-of-view study of the Eagle Nebula with the Fourier transform imaging spectrograph SITELLE at CFHT," **635**, A111 (Mar. 2020).

[18] Alarie, A. and Drissen, L., "A multispectral analysis of the northeastern shell of IC 443," **489**, 3042–3058 (Nov. 2019).

[19] Martin, T., Milisavljevic, D., and Drissen, L., "3D mapping of the Crab Nebula with SITELLE - I. Deconvolution and kinematic reconstruction," **502**, 1864–1881 (Apr. 2021).

[20] Bisaria, D., Spekkens, K., Huang, S., Hallenbeck, G., and Haynes, M. P., "Non-circular flows in HIghMass galaxies in a test of the late accretion hypothesis," **509**, 100–113 (Jan. 2022).

[21] Karera, P., Drissen, L., Martel, H., Iglesias-Páramo, J., Vilchez, J. M., Duc, P.-A., and Plana, H., "The interacting pair of galaxies Arp 82: integral field spectroscopy and numerical simulations," **514**, 2769–2792 (Aug. 2022).

[22] Lu, A., Boyce, H., Haggard, D., Bureau, M., Liang, F.-H., Liu, L., Choi, W., Cappellari, M., Chemin, L., Chevance, M., Davis, T. A., Drissen, L., Elford, J. S., Gensior, J., Kruijssen, J. M. D., Martin, T., Massé, E., Robert, C., Ruffa, I., Rousseau-Nepton, L., Sarzi, M., Savard, G., and Williams, T. G., "WISDOM project - XI. Star Formation Efficiency in the Bulge of the AGN-host Galaxy NGC 3169 with SITELLE and ALMA," (June 2022).

[23] Rousseau-Nepton, L., Martin, R. P., Robert, C., Drissen, L., Amram, P., Prunet, S., Martin, T., Moumen, I., Adamo, A., Alarie, A., Barmby, P., Boselli, A., Bresolin, F., Bureau, M., Chemin, L., Fernandes, R. C., Combes, F., Crowder, C., Della Bruna, L., Duarte Puertas, S., Egusa, F., Epinat, B., Ksoll, V. F., Girard, M., Gómez Llanos, V., Gouliermis, D., Grasha, K., Higgs, C., Hlavacek-Larrondo, J., Ho, I. T., Iglesias-Páramo, J., Joncas, G., Kam, Z. S., Karera, P., Kennicutt, R. C., Klessen, R. S., Lianou, S., Liu, L., Liu, Q., de Amorim, A. L., Lyman, J. D., Martel, H., Mazzilli-Ciraulo, B., McLeod, A. F., Melchior, A. L., Millan, I., Mollá, M., Momose, R., Morisset, C., Pan, H. A., Pati, A. K., Pellerin, A., Pellegrini, E., Pérez, I., Petric, A., Plana, H., Rahner, D., Ruiz Lara, T., Sánchez-Menguiano, L., Spekkens, K., Stasińska, G., Takamiya, M., Vale Asari, N., and Vílchez, J. M., "SIGNALS: I. Survey description," **489**, 5530–5546 (Nov. 2019).

[24] Martin, T. B., Drissen, L., and Melchior, A.-L., "A SITELLE view of M31's central region - I. Calibrations and radial velocity catalogue of nearly 800 emission-line point-like sources," **473**, 4130–4149 (Jan. 2018).

[25] Rousseau-Nepton, L., Robert, C., Martin, R. P., Drissen, L., and Martin, T., "NGC628 with SITELLE: I. Imaging spectroscopy of 4285 H II region candidates," **477**, 4152–4186 (Feb. 2018).

[26] Pellegrini, E. W., Rahner, D., Reissl, S., Glover, S. C. O., Klessen, R. S., Rousseau-Nepton, L., and Herrera-Camus, R., "WARPFIELD-EMP: The self-consistent prediction of emission lines from evolving H II regions in dense molecular clouds," **496**, 339–363 (July 2020).

[27] Moumen, I., Robert, C., Devost, D., Martin, R. P., Rousseau-Nepton, L., Drissen, L., and Martin, T., "3D optical spectroscopic study of NGC 3344 with SITELLE: I. Identification and confirmation of supernova remnants," **488**, 803–829 (Sept. 2019).

[28] Duarte Puertas, S., Iglesias-Páramo, J., Vilchez, J. M., Drissen, L., Kehrig, C., and Martin, T., "Searching for intergalactic star forming regions in Stephan's Quintet with SITELLE. I. Ionised gas structures and kinematics," **629**, A102 (Sept. 2019).

[29] Duarte Puertas, S., Vilchez, J. M., Iglesias-Páramo, J., Drissen, L., Kehrig, C., Martin, T., Pérez-Montero, E., and Arroyo-Polonio, A., "Searching for intergalactic star forming regions in Stephan's Quintet with SITELLE. II. Physical properties and metallicity," **645**, A57 (Jan. 2021).

[30] Gendron-Marsolais, M., Hlavacek-Larrondo, J., Martin, T. B., Drissen, L., McDonald, M., Fabian, A. C., Edge, A. C., Hamer, S. L., McNamara, B., and Morrison, G., "Revealing the velocity structure of the filamentary nebula in NGC 1275 in its entirety," **479**, L28–L33 (Sept. 2018).

[31] Liu, Q., Yee, H. K. C., Drissen, L., Sivanandam, S., Pintos-Castro, I., Alcorn, L. Y., Hsieh, B.-C., Lin, L., Lin, Y.-T., Muzzin, A., Noble, A., and Old, L., "SITELLE Hα Imaging Spectroscopy of z $\sim$ 0.25 Clusters: Emission-line Galaxy Detection and Ionized Gas Offset in Abell 2390 and Abell 2465," **908**, 228 (Feb. 2021).

[32] Edwards, L. O. V., Durret, F., Márquez, I., and Zhang, K., "Efficient Detection of Emission-line Galaxies in the Cl0016+1609 and MACSJ1621.4+3810 Supercluster Filaments Using SITELLE," **161**, 255 (June 2021).